Green synthesis of iron-organic framework Fe-BTC using direct ultrasound to remove methylene blue dye

Nam Ho Phung Khac

[1]Institute of Chemistry and Materials, No. 17 Hoang Sam Street, Cau Giay District, Ha Noi, Vietnam

Email: homyhu@gmail.com

Abstract— Metal-organic framework materials (MOFs) comprise organic bridges and metal centers (as connection points). MOFs have unique properties such as crystal structure, large specific surface area, flexible structural framework, and can change the size and shape of pores and diverse chemical functional groups inside the pores. In this study, metal-organic framework materials based on iron (Fe) and the organic ligand H_3BTC were successfully synthesized by ultrasonic method and evaluated for their ability to remove MB dye through Investigate the effects of MB concentration, pH, isotherm model, and adsorption kinetics. With a size of about 100 - 200 nm and an excitation wavelength in the ultraviolet region, the synthesized material shows potential in environmental treatment when the adsorption efficiency reaches over 60% after just 10 minutes and over 80% both processes under sunlight conditions. In addition, the synthesized material is also evaluated to have selective adsorption with Methylene Blue dye.

Keywords—Metal-organic frameworks, removing dye, methylene blue, treatment wastewater.

I. INTRODUCTION

In recent years, industrial wastewater from textile industries containing many organic pigments has become a severe problem in developing countries [1]. Most organic colors are chemically stable, difficult to decompose, and can destroy the environment if not handled properly [2]. In particular, Methylene Blue (MB) is a popular organic colorant in the textile industry [3]. This type of organic pigment has a long-term impact on the environment due to its ability to block sunlight from entering the aquatic environment, thereby affecting living organisms. On the other hand, for public health, MB can cause eye burns and permanent damage. It produces a burning sensation if swallowed, leading to nausea [4]. Therefore, advanced technology to treat wastewater from dye production is exciting. Up to now, a series of wastewater treatment technologies have been developed, such as biodegradation [5], physical adsorption [6], chemical reaction [7], etc. In advanced oxidation processes, photocatalytic degradation technology is highly effective in decomposing organic pigments into less toxic or biodegradable molecules or even minerals. Transform them into less harmful

substances such as CO_2 and H_2O under sunlight and have more economical treatment costs [8, 9].

The current potential type of material for environmental treatment based on adsorption and photocatalysis mechanisms is organometallic framework materials (MOFs) [10]. Compared with traditional system photocatalysts, MOF materials have many advantages in improving photocatalytic efficiency due to their high topology and surface area, which are favorable for the rapid migration and accumulation of organic dye molecules [11]. In particular, iron-based metal-organic framework materials (Fe-MOFs), an essential branch of MOFs, not only have topological properties and a high specific surface area similar to many other MOF materials but are also more environmentally friendly [12]. The methods for synthesizing Fe-MOF materials are very diverse. Among those methods, the solvothermal method is mainly used, but ultrasound-based synthesis is preferred because it saves synthesis time and energy [13]. During ultrasound, periodic mechanical vibrations with large wavelengths interact with the liquid, creating sudden pressure fluctuations. The bubbles forming, growing, and collapsing inside these points lead to localized hot zones

with extremely high temperatures and pressures, creating favorable conditions for chemical reactions in a solution containing precursors and forming material structures [14].

In this study, metal-organic framework materials based on iron (Fe) were synthesized by direct ultrasonic method with green water solvent. It was evaluated for structural characteristics and decomposition ability with MB organic pigment. Among them, the organic ligand 1,3,5-benzene dicarboxylate (BTC), one of the most versatile ligands for synthesizing MOFs thanks to its different binding sites [15], was used to construct MOFs. Build the structural framework of the material.

II.   EXPERIMENTS

Chemicals

Iron (III) chloride hexahydrate ($FeCl_3.6H_2O$, 99%, Xilong, China); 1,3,5-benzenetricarboxylic acid (H_3BTC, 98%, Macklin, China); Ethanol (C_2H_6O, 95%, Macklin, China); Sodium hydroxide (NaOH, 99%, Macklin, China); Hydrochloric acid (HCl, 37%, Xilong, China); distilled water.

Synthesis of Fe-BTC material

First, 5.4 grams of $FeCl_3.6H_2O$ material were wholly dissolved in 200 ml of distilled water, and 2.8 grams of H_3BTC material were added and then stirred well on a magnetic stirrer at a speed of 400 rpm. After stirring for 30 minutes, the solution system was sonicated with an operating capacity of 1440W run/rest pulse of 10 seconds/5 seconds for 10 minutes. The product was then centrifuged, the solution removed, washed several times with ethanol, and then dried at 120 °C for 6 hours.

Characterizations

Scanning electron microscopy Hitachi S-4600 was employed to observe particle size and morphology. An X'Pert PRO PANalytical instrument with a radiation source of 0.154 nm CuK_α has obtained XRD patterns for all samples. Fourier transform infrared spectroscopy (FTIR, TENSOR II, Bruker) was used to investigate the surface functional groups of the MOF material. The N_2 adsorption isotherm at 77 K using a BET TriStar II Plus 377 was employed to calculate the surface area of the material.

Removal of methylene blue

The experiments were conducted with the ratio of Fe-BTC material to the amount of MB solution of 0.5 g per litter. The Fe-BTC material and the MB solution were put into a transparent glass tube, sealed with a tight cap, and put into a closed dark box to study the MB adsorption capacity of the material. For the experiment to evaluate the

simultaneous adsorption-catalysis ability, the tube is put under simulated sunlight by Xenon lamp. After the time needed to survey, filter out the material from the solution to analyze the MB concentration by UV-Vis photometric method on a UV-Vis DV-8200 device (Drawell).

The equation for the determination of MB concentration was built as follows:

$$C = 6.2933Abs + 0.12955 \qquad (1)$$

with ($\lambda = 664$ nm, $R^2 = 0.9983$).

Where, C is the concentration of MB in the solution, mg/L. Abs is the intensity of light absorption. R^2 is the correlation coefficient of the empirically constructed standard curve equation.

The formula calculated the MB removal efficiency of the material:

$$H\ (\%) = \frac{(C_0 - C_t)}{C_0} \times 100 \qquad (2)$$

The adsorption capacity was calculated according to the procedure:

$$q_t\ (mg/g) = \frac{V \times (C_0 - C_t)}{m} \qquad (3)$$

Where, C_0, C_t are MB (mg/L) concentrations initially and at time t; V is the volume of MB solution (L); m is the mass of material Fe-BTC (g).

III.   RESULTS AND DISCUSTION

Characterization of Fe-BTC
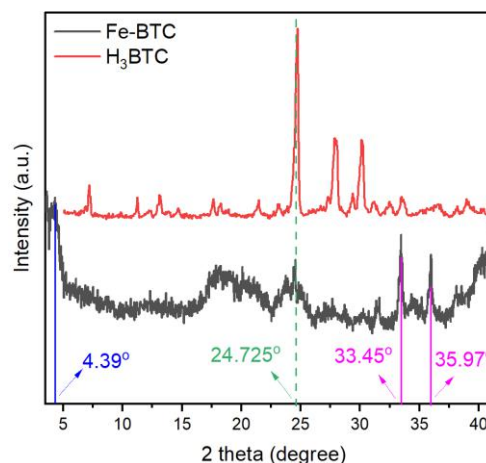
Fig. 1: X-ray diffraction pattern of the Fe-BTC by ultrasound.

The structural phase characteristics of the synthesized material are shown in Fig. 1. The signal intensity of the XRD spectrum shows that the material has poor

crystallization. However, the presence of H$_3$BTC material at position 24.725º can be assessed initially. Besides, a unique diffraction peak appears at position 4.39º, corresponding to the (001) lattice the monoclinic crystal system in the material Fe$_4$O$_{12}$C$_{116}$H$_{128}$ [16]. Although no characteristic peak exists at the angular position 5º to 15º, the synthesized material exhibits a broadened peak from 16º to 22.5º. The impact on this structure may be due to the nano size of the material [17] or the existence of some α-Fe$_2$O$_3$ particles [18]. The 33.45º and 35.97º peaks correspond to the standard spectrum 96-901-4881.

The morphology of the synthesized material is shown in Fig.2. The particle material was evaluated with sizes ranging from 100 to 200 nm. At the same time, the material system agglomerates together due to the influence of the magnetic material α-Fe$_2$O$_3$ [19], but this accumulation is not significant.
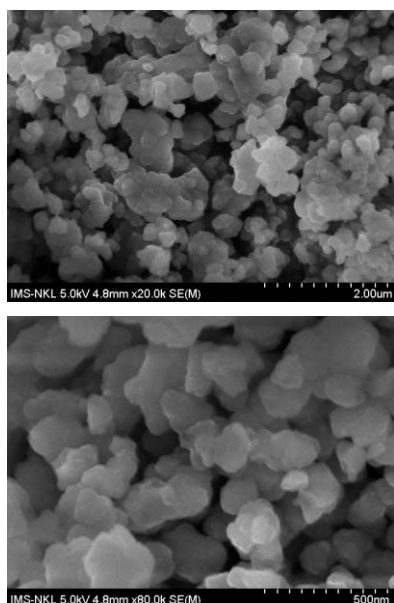
Fig. 2: Scanning electron microscopy (SEM) images of Fe-BTC by ultrasound.

The FTIR spectrum of the synthesized material and H$_3$BTC is shown in Fig. 3. In the spectrum of the Fe-BTC material, a broadened peak appears at the wavenumber position of about 3400 cm^{-1}, representing the OH group vibration of the molecules. Water molecules are adsorbed on the surface [20]. The peaks at positions 1627 cm^{-1} and 1574 cm^{-1} represent asymmetric stretching vibrations of the carboxylate group in the organic ligand BTC. In addition, the symmetric vibrations of this group are also shown at two peaks at 1376 cm^{-1} and 1450 cm^{-1}. The peaks at wave number 710 - 757 cm^{-1} represent the CH bond of the aromatic ring. In particular, the peaks at positions 459 - 479 cm^{-1} represent the Fe-O vibrations of the material [17, 20, 21].
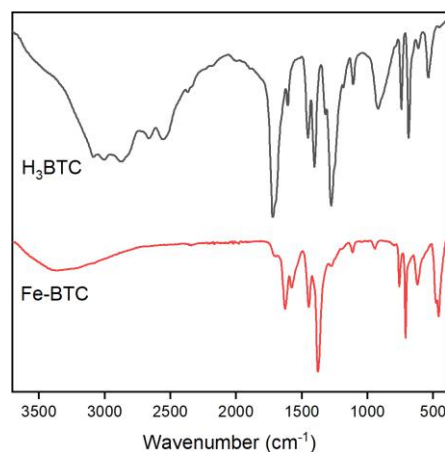
Fig. 3: FTIR spectra of Fe-BTC by ultrasound.

N$_2$ adsorption isotherm research is used to predict the adsorption capacity of Fe-BTC material. The N$_2$ adsorption-desorption diagram of Fe-BTC is recorded in Fig. 4. The BET surface area of the Fe-BTC sample was 259.846 m^2/g.
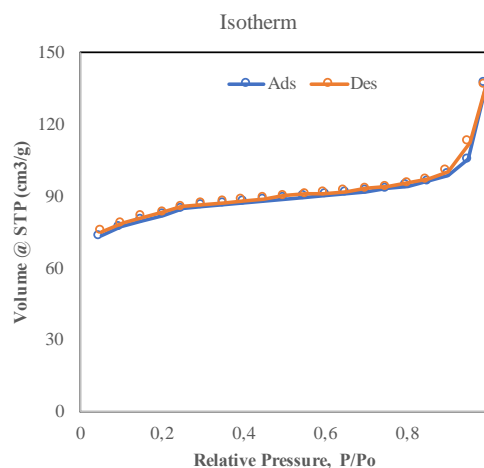
Fig. 4: FTIR spectra of Fe-BTC by ultrasound.
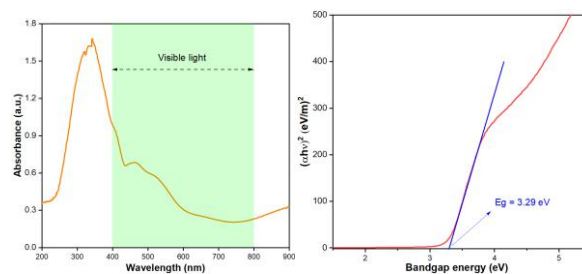
Fig. 5: The UV-Vis spectrum of Fe-BTC by ultrasound.

From the characteristic properties analyzed above, the research team confirmed that they have successfully synthesized the metal-organic framework material Fe using the organic ligand BTC. On the other hand, for

applications in the field of adsorption and photocatalysis, parameters related to the optical band gap of the material are critical to determine the optical activity of the material [22]. Using the Tauc method [23], the calculated width energy is about 3.29 eV (Fig. 5), equivalent to the excitation wavelength in the ultraviolet region.

Removal of methylene blue

The material's ability to process MB over time in dark conditions (adsorption) and sunlight conditions (adsorption - photocatalysis) with a Fe-BTC mass of 10 mg per 20 mL of MB solution with a concentration of 10 mg/L is shown in Fig. 6. In general, the efficiency of photocatalytic adsorption treatment is much higher than that of adsorption treatment, about 16 - 31% for each measurement time. For adsorption-photocatalytic treatment, the efficiency reaches 61.48% after 10 minutes and reaches adsorption equilibrium after 60 minutes with an efficiency of about 86%. Meanwhile, adsorption treatment got 30% after 10 minutes and nearly 70% after 60 minutes.
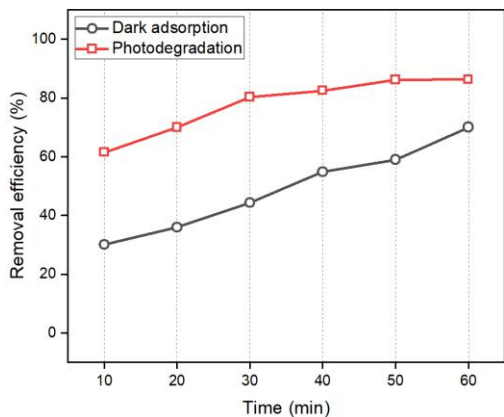
Fig. 6: Adsorption performance of Fe-BTC by ultrasound.

The influence of pH on MB removal efficiency was evaluated in the range from 3 to 11 (adjusting the pH of the stock MB solution with 1 M HCl and 1 M NaOH solutions). The chart evaluating the influence of pH (Fig. 7a) shows that MB treatment efficiency under light conditions is significantly higher than under dark conditions. At the same time, through analysis of Fig. 7b, it is found that the material achieves the highest MB treatment efficiency at pH = 7 in dark conditions. The equilibrium MB removal efficiency increases when pH increases from 3 to 7 because, in acidic environments, many H^+ ions exist that can compete with harmful cations separated from MB, reducing adsorption performance [24]. On the other hand, when the pH value increases from 7 to 11, the adsorption efficiency and capacity decrease due to the reaction between $MB-S^+Cl$ and NaOH in the solution to form a solution containing $MB-S^+OH$ and NaCl. NaCl

salt has been shown to reduce the adsorption process of $MB-S^+OH$ on the surface of adsorbent materials [25]. The treatment efficiency is similar for lighting conditions when increasing pH from 3 to 7. However, when increasing the pH value from 7 to 9, the treatment efficiency drops sharply from 85.1% to about 59.0 % and then increases significantly to 87.67% at pH 11. It can be explained by the fact that in a solution of pH 9 and under solid illumination, the reaction between MB and NaOH occurs strongly, causing the adsorption efficiency to decrease. However, when increasing the pH to 11 and under the influence of solid light, MB's dimerization process occurs, shifting the maximum peak from 662 nm to about 610 nm (Fig. 7c).
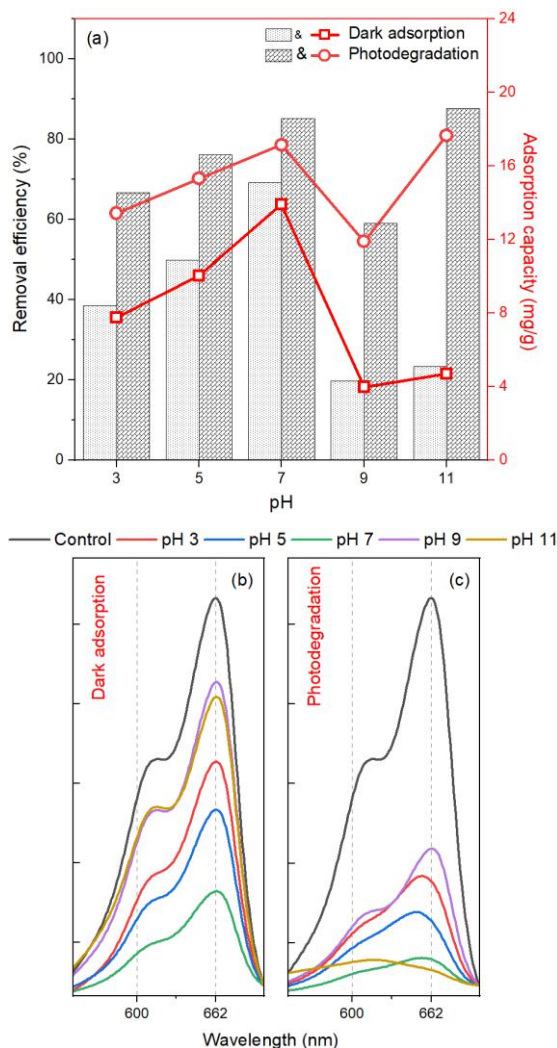
Fig. 7: Effect of pH on the ability to treat MB (a), UV-Vis spectrum of MB solution after adsorption treatment (b), and adsorption - photocatalysis (c).

Three isotherm equations are applied to study the interaction between the adsorbent and adsorbate: Langmuir, Freunlich, and Temkin. The correlation coefficient R^2 values in Fig. 8 show that the adsorption

data of FeBTC material is in good agreement with the Freunlich model. Proving that the adsorption process is multilayer on heterogeneous surfaces [26]. In addition, the parameters of the models are summarized in Table 1.

Freunlich	$\ln q_e = \ln K_F + \frac{1}{n} \ln C_e$	n = 3,1656 K_F = 29.20452 (mg/g) R^2 = 0.9968
Temkin	$q_e = B_t \ln K_t + B_t \ln C_e$	B_t = 12 , 1745 (J/mol) K_t = 14 .02186 (L/mg) R^2 = 0.9479

The adsorption kinetics of the material were studied through first- and second-order kinetic models at an initial MB concentration of 10 mg/L. Based on the correlation coefficient of the two linear lines, it is found that the material's kinetic model is more compatible with the first-order kinetic model than the second-order kinetic model (Fig. 9).

Fig. 8: Adsorption isotherm of the Fe-BTC toward MB.

Table 1: Adsorption isotherm parameters of Fe-BTC by ultrasound.

Model	Equation	Parameters
Langmuir	$\dfrac{C_e}{q_e} = \dfrac{1}{K_L \cdot q_m} + \dfrac{C_e}{q_m}$	q_{max} = 57.30659 (mg/g) K_L = 1.804 (L/mg) R_L = 0.052506 R^2 = 0.9507
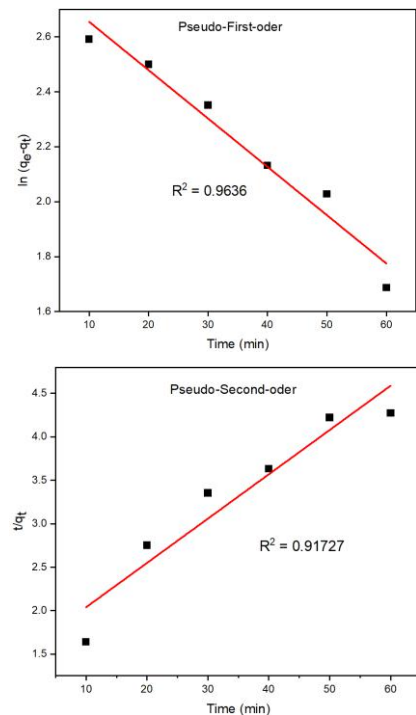
Fig. 9: The kinetic models of Fe-BTC adsorption toward MB.
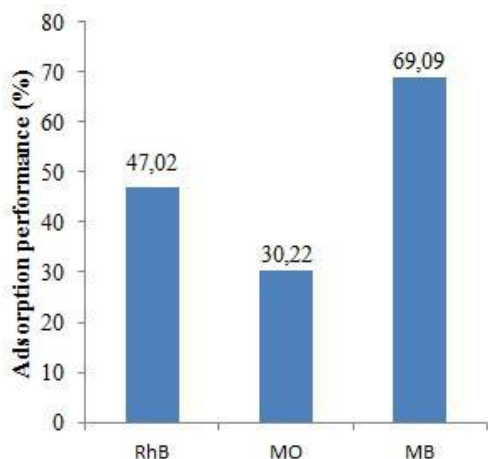
Fig. 10: Adsorption performance of Fe-BTC materials for different dyes after 60 minutes.

Finally, to evaluate the adsorption selectivity, two solutions containing the dyes Methyl Orange (MO) and Rhodamine B (RhB) with the same volume of 20 mL and concentration of 10 mg/L were tested during the adsorption 60-minute period. Based on Fig. 10, it is seen that Fe-BTC material can adsorb dye MB more optimally than the others because the adsorption efficiency after 60 minutes with RhB and MO is 47.02% and 30.22%, respectively. Meanwhile, under the same survey conditions, the MB adsorption efficiency of this material is 69.09%. Survey results show that Fe-BTC material can adsorb all three families of dyes with decreasing levels in the order MB > RhB > MO.

IV.   CONCLUSION

This research has successfully synthesized the iron-organic framework material with water as a green solvent by direct ultrasound. Fe-BCT in granular form with a size of about 100 - 200 nm determined the excitation light wavelength of the material in the ultraviolet region. Experimental evaluation of the ability to decompose MB pigment shows that the material has an adsorption efficiency of up to 60% in 60 minutes in dark conditions and over 80% in 60 minutes in sunlight conditions. The adsorption process of the determined material is better compatible with the Freunlich isotherm model and first-order adsorption kinetics. In addition, the material also shows better adsorption selectivity with MB than MO and RhB.

ACKNOWLEDGEMENTS

REFERENCES

[1] Tianqi Liu, Chukwunonso O. Aniagor, Marcel I. Ejimofor, Matthew C. Menkiti, Yakubu M. Wakawa, Jie Li, Rachid Ait Akbour, Pow-Seng Yap, Sie Yon Lau, Jaison Jeevanandam (2023). Recent developments in the utilization of modified graphene oxide to adsorb dyes from water: A review. Journal of Industrial and Engineering Chemistry, 117, 21-37.

[2] F S. Banerjee, P. Benjwal, M. Singh, KKJAss Kar (2018). Graphene oxide (rGO)-metal oxide (TiO_2/Fe_3O_4) based nanocomposites for the removal of methylene blue. Applied Surface Science, 439, 560-568.

[3] Z. Mengting, TA Kurniawan, S. Fei, T. Ouyang, MHD Othman, M. Rezakazemi, SJEP Shirazian (2019). Applicability of $BaTiO_3$/graphene oxide (GO) composite for enhanced photodegradation of methylene blue (MB) in synthetic wastewater under UV–vis irradiation. Environmental Pollution, 255(Part1), 113182.

[4] R. Al-Tohamy, SS Ali, F. Li, KM Okasha, YAG Mahmoud, T. Elsamahy, H. Jiao, Y. Fu, J. Sun (2022). A critical review on the treatment of dye-containing wastewater: Ecotoxicological and health concerns of textile dyes and possible remediation approaches for environmental safety. Ecotoxicology and Environmental Safety, 231, 113160.

[5] K. Qi, Z. Li, C. Zhang, X. Tan, C. Wan, X. Liu, L. Wang, D.J. Lee (2020). Biodegradation of real industrial wastewater containing ethylene glycol by using aerobic granular sludge in a continuous-flow reactor: Performance and resistance mechanism. Biochemical Engineering Journal, 161, 107711.

[6] C. Yin, C. Xu, Y. Jia, W. Sun, C. Wang, G. Zhou, M. Xian (2019). Insight into highly efficient removal of sulfonic acid pollutants by a series of newly-synthesized resins from aqueous media: Physical & chemical adsorption. Journal of the Taiwan Institute of Chemical Engineers, 95, 383-392.

[7] J. Chakraborty, I. Nath, S. Song, S. Mohamed, A. Khan, PM Heynderickx, F. Verpoort (2019). Porous organic polymer composites as surging catalysts for visible-light-driven chemical transformations and pollutant degradation. Journal of Photochemistry and Photobiology C: Photochemistry Reviews, 41, 100319

[8] I. Khan, K. Saeed, N. Ali, I. Khan, B. Zhang, M. Sadiq (2020). Heterogeneous photodegradation of industrial dyes: An insight to different mechanisms and rate affecting parameters. Journal of Environmental Chemical Engineering 8(5), 104364.

[9] C. Feng, Z. Chen, J. Jing, J. Hou (2020). The photocatalytic phenol degradation mechanism of Ag-modified ZnO nanorods. Journal of Materials Chemistry C, 8(9), 3000-3009.

[10] V. García-Salcido, P. Mercado-Oliva, JL Guzmán-Mar, BI Kharisov, L. Hinojosa-Reyes (2022). MOF-based composites for visible-light-driven heterogeneous photocatalysis: Synthesis, characterization and environmental application studies. Journal of Solid State Chemistry, 307, 122801.

[11] Y. Bai, S. Zhang, S. Feng, M. Zhu, S. Ma (2020). The first ternary Nd-MOF/GO/Fe_3O_4 nanocomposite exhibiting an

excellent photocatalytic performance for dye degradation. Dalton Transactions, 49(31), 10745-10754.

[12] G. Zhu, S. Wang, Z. Yu, L. Zhang, D. Wang, B. Pang, W. Sun (2019). Application of Fe-MOFs in advanced oxidation processes. Research on Chemical Intermediates 45(7) 3777-3793.

[13] J. Joseph, S. Iftekhar, V. Srivastava, Z. Fallah, EN Zare, M. Sillanpää (2021). Iron-based metal-organic framework: Synthesis, structure and current technologies for water reclamation with deep insight into framework integrity. Chemosphere, 284, 131171.

[14] C. Vaitsis, G. Sourkouni, C. Argirusis (2019). Metal Organic Frameworks (MOFs) and ultrasound: A review. Ultrasonics Sonochemistry, 52, 106-119.

[15] [15] A. Sarkar, A. Adhikary, A. Mandal, T. Chakraborty, D. Das (2020). Zn-BTC MOF as an Adsorbent for Iodine Uptake and Organic Dye Degradation. Crystal Growth & Design, 20(12) ,7833-7839.

[16] JA Carmona-Negrón, A. Santana, AL Rheingold, E. Meléndez (2019). Synthesis, structure, docking and cytotoxic studies of ferrocene–hormone conjugates for hormone-dependent breast cancer application. Dalton Transactions, 48(18), 5952-5964.

[17] P. Horcajada, S. Surblé, C. Serre, D.-Y. Hong, Y.-K. Seo, J.-S. Chang, J.-M. Grenèche, I. Margiolaki, G. Férey (2007). Synthesis and catalytic properties of MIL-100(Fe), an iron(iii) carboxylate with large pores. Chemical Communications, (27), 2820-2822.

[18] N. Armon, E. Greenberg, E. Edri, A. Kenigsberg, S. Piperno, O. Kapon, O. Fleker, I. Perelshtein, G. Cohen-Taguri, I. Hod, H. Shpaisman (2019). Simultaneous laser-induced synthesis and micro-patterning of a metal organic framework. Chemical Communications, 55(85), 12773-12776

[19] V. Ramalingam, M. Harshavardhan, S. Dinesh Kumar, S. Malathi Devi (2020). Wet chemical mediated hematite α-Fe2O3 nanoparticles synthesis: Preparation, characterization and anticancer activity against human metastatic ovarian cancer. Journal of Alloys and Compounds, 834(5), 155118-155128.

[20] NK Gupta, J. Bae, KS Kim (2021). Iron-organic frameworks-derived iron oxide adsorbents for hydrogen sulfide removal at room temperature. Journal of Environmental Chemical Engineering, 9(5), 106195.

[21] AA Castañeda Ramírez, E. Rojas García, R. López Medina, JL Contreras Larios, R. Suárez Parra, AM Maubert Franco (2021). Selective Adsorption of Aqueous Diclofenac Sodium, Naproxen Sodium, and Ibuprofen Using a Stable Fe3O4–FeBTC Metal–Organic Framework. Materials, 14(9), 2293.

[22] P. Makuła, M. Pacia, WJTjopcl Macyk (2018). How To Correctly Determine the Band Gap Energy of Modified Semiconductor Photocatalysts Based on UV–Vis Spectra. The Journal of Physical Chemistry Letters, 9(23), 6814-6817.

[23] K. Fabrizio, KN Le, AB Andreeva, CH Hendon, CKJAML Brozek (2022). Determining Optical Band Gaps of MOFs. ACS Materials Letters, 4(3), 457-463.

[24] Y. Xu, J. Jin, X. Li, C. Song, H. Meng, X. Zhang (2016). Adsorption behavior of methylene blue on Fe3O4-embedded hybrid magnetic metal–organic framework. Desalination and Water Treatment, 57(52), 25216-25225.

[25] JO Amode, JH Santos, Z. Md. Alam, AH Mirza, CC Mei (2016). Adsorption of methylene blue from aqueous solution using untreated and treated (Metroxylon spp.) waste adsorbent: equilibrium and kinetics studies. International Journal of Industrial Chemistry, 7(3), 333-345.

[26] VO Shikuku, T. Mishra (2021). Adsorption isotherm modeling for methylene blue removal onto magnetic kaolinite clay: a comparison of two-parameter isotherms. Applied Water Science, 11(6), 103.